ISPRS Annals of the Photogrammetry, Remote Sensing and Spatial Information Sciences, Volume X-M-1-2023
29th CIPA Symposium "Documenting, Understanding, Preserving Cultural Heritage:
Humanities and Digital Technologies for Shaping the Future", 25–30 June 2023, Florence, Italy

VALIDATION OF FULL-RESOLUTION DINSAR-DERIVED VERTICAL DISPLACEMENT IN CULTURAL HERITAGE MONITORING: INTEGRATION WITH GEODETIC LEVELLING MEASUREMENTS

R. Eskandari *, M. Scaioni

Dept. of Architecture, Built Environment and Construction Engineering, Politecnico di Milano, via Ponzio 31, 20133 Milano, Italy - rasoul.eskandari@polimi.it, marco.scaioni@polimi.it

KEY WORDS: Synthetic Aperture Radar, Full-Resolution DInSAR, Weighted Localized Vertical Displacement Extraction, Geodetic Levelling Measurements, Cultural Heritage

ABSTRACT:

Towards revealing the potential of satellite Synthetic Aperture Radar (SAR) Interferometry (InSAR) for efficient detection and monitoring of Cultural Heritage (CH) encouraging resilient built CH, this study is devoted to the validation of InSAR-derived vertical displacements with a full-resolution perspective taking advantage of high-precision geodetic levelling measurements. Considering the Cathedral of Como, northern Italy, as the case study, two different Persistent Scatterer Interferometry (PSI) techniques have been applied to Cosmo-SkyMed high-resolution SAR images acquired in both ascending and descending orbit tacks within the time interval of 2010-2012. Besides using the simplified approach for obtaining the vertical displacement velocity from Line of Sight (LOS) velocity, a weighted, localized, multi-track Vertical Displacement Extraction (VDE) approach is proposed and evaluated, which uses the technical outcome of Differential InSAR (DInSAR) and spatial information. The results, using a proper PSI technique, showed that the accuracy level of extracted vertical displacement velocities in a full-resolution application is ca. 0.6 [mm/year] with a dense concentration of InSAR-Levelling absolute errors lower than 0.3 [mm/year] which are reliable and reasonable levels based on the employed validation framework in this study. Also, the weighted localized VDE can significantly decrease the InSAR-Levelling errors, adding to the reliability of the InSAR application for CH monitoring and condition assessment in practice.

1. INTRODUCTION

Built heritage and archaeological sites are prone to tangible and intangible damages caused by progressive ground deformation due to earthquakes, anthropogenic/natural subsidence, landslide, etc. The high physical and systemic vulnerability against this geohazard (Themistocleous et al., 2016) and the unique socio-economic values (Rudokas et al., 2019) of these cultural assets particularly demand proper frameworks for assessment and monitoring purposes. In this context, the framework requires a high level of interdisciplinarity and reliability for better identification of the current condition and evolutionary processes to support the planning of conservation and mitigation measures towards resilient Cultural Heritage (CH).

Among the Structural Health Monitoring (SHM) techniques for measuring deformations, performing on-site measurements is characterized by being expensive, time-consuming, and demanding in terms of necessary expert operators (Yang et al., 2022; Scaioni et al., 2018), which leads to low operational frequency. The limited number of measurement points (e.g. in the case of optical levelling measurements and LVDT sensors) and low level of precision (e.g. in the case of Terrestrial Laser Scanning (TLS) (Wojtkowska et al., 2021)) are other disadvantages of these techniques.

On the other hand, Synthetic Aperture Radar (SAR) Interferometry (InSAR), as a powerful remote sensing technology, has been proven to be able to partially, but effectively, overcome these challenges in different scales of application. Persistent Scatterer InSAR (PS-InSAR) (Ferretti et al., 2000, 2001) was the first pioneering technique introduced in the concept of Persistent Scatterer (PS) Interferometry (PSI), which was followed by further developments, such as Interferometric Point Target Analysis (IPTA) (Werner et al., 2003), PS Pairs (PSP) (Costantini et al., 2008), and Quasi-PS-InSAR (namely partially coherent targets) (Perissin and Wang, 2012). The availability of Multi-Temporal (MT) SAR images, acquired in relatively short time spans and from slightly different satellite positions, makes these techniques able to estimate useful information (such as height relative to the ground, deformation trend, and seasonal displacements) corresponding to the sensor-friendly targets on the earth surface through Differential InSAR (DInSAR). For a comprehensive and complete review, refer to (Crosetto et al., 2016; Ho Tong Minh et al., 2020).

Among the broad field of InSAR applications, Archeological and Cultural Heritage (ACH) and historic areas are involved in a special class of application which has increasingly gained the attention of researchers in the last decade. The low to medium resolution (C-band) SAR images (such as ERS1/2 (Tapete et al., 2012; Eskandari and Scaioni, 2023), Envisat (Tapete et al., 2013), and Sentinel-1 (Tzouvaras et al., 2019; Moise et al., 2021), etc.) are reported to have the capability of deformation detection from large-scale historic sites to local-scale of multiple buildings (in some cases, few measure points on a single building with a large plan (Karila et al., 2013)).

This limited number of target points may represent the overall phenomenon progressing over the heritage of interest, therefore, they may be sufficient for monitoring, decision-making, and taking actions (Tapete and Cigna, 2017b). However, the satellite missions such as Cosmo-SkyMed (CSK) and TerraSAR-X launched by the European Space Agency (ESA) are providing high and very high-resolution SAR images (X-band), practically from the early 2010s, which have opened the doors to monitoring and condition assessment of built CH with a high level of detail. Here, a brief review of the recent relevant applications is provided.

In the case of using CSK, Cavalagli et al. have established the relation between the InSAR-derived information and the outcomes of on-site monitoring systems implemented on some

* Corresponding author

This contribution has been peer-reviewed. The double-blind peer-review was conducted on the basis of the full paper.
https://doi.org/10.5194/isprs-annals-X-M-1-2023-79-2023 | © Author(s) 2023. CC BY 4.0 License.

built heritage of Gubbio, Italy (Cavalagli et al., 2019; Cavalagli et al., 2021). Bozzano et al. have used the deformation history of the PSs detected on a historic Monument in Rome, Italy, to retrieve a comprehension of the deformations and damages to the asset, supported by geological data (Bozzano et al., 2020). By considering two case studies of CH, Berto et al. have evaluated the reliability of PS information in this class of application (Berto et al., 2021). Tapete et al. have fully investigated the CSK capabilities and applications developed and implemented from 2017 to 2019, specifically for the detection and assessment of archaeological and heritage sites, using SAR images acquired in both StripMap and Spotlight image modes (3m and 1m spatial resolution, respectively) (Tapete and Cigna, 2019). The recent exploitation of TerraSAR-X images integrated with other techniques for monitoring CH can be seen in (Chen et al., 2021; Chen et al., 2022). For a complete review of the primitive applications of space-borne InSAR for ACH, interested readers may refer to (Tapete and Cigna, 2017a; Chen et al., 2017; Lasaponara and Masini, 2020).

According to the literature, there is always the need for further investigation into the reliability and precision of information obtained by InSAR. Furthermore, addressing how to overcome the encountered challenges and evaluating the further potential of InSAR for monitoring ACH play an important role in encouraging the transition of satellite InSAR monitoring from research to practice. In this letter, using different PSI algorithms implemented in the SARPROZ software package (Perissin et al., 2011), the reliability of InSAR-detected vertical displacements (properly extracted using simplified and proposed vertical component extraction techniques) over Cathedral of Como, Northern Italy, is evaluated through integration with the precise levelling measurements. The results particularly contribute to the performance assessment of fully-exploited InSAR using high-resolution SAR images for detection and monitoring of cultural heritage, by assessing the modified framework for validation purposes and determining an accuracy level for this type of deformation monitoring.

2. CASE STUDY AND MATERIALS

2.1 Cathedral of Como, Italy

The Cathedral of Como (in Italian: Duomo di Como) placed at the historic centre of Como, northern Italy, is considered as the case study of this work. Como town located adjacent to the Lake of Como is known to be subjected to various rates of natural/anthropogenic subsidence (or uplift) which has been evaluated and monitored through optical levelling operations in the past and satellite InSAR in recent years, to shed light on the triggering factors of the phenomenon (Nappo et al., 2020), the corresponding effects on the built historic area (Nappo et al., 2021), and hydro-geotechnical settings of the area (Bajni et al., 2019) via multidisciplinary approaches. Also, through a statistical approach, the PSI measurements using the archive of medium-resolution ERS 1/2 SAR images have been validated using the precise historic vertical displacement rates collected from the urban-scale levelling network of the Como area (Eskandari and Scaioni, 2023).

2.2 Raw Data: InSAR and Levelling

To perform the multitemporal InSAR analysis, SAR stacks of Single-Look Complex (SLC) products acquired by Cosmo-SkyMed (CSK) satellite mission in the Stripmap HIMAGE mode (spatial resolution of 3 meters) orbiting in both tracks (ascending and descending) are used, and the corresponding details are listed in Table 1. The external data implemented for the DInSAR processing include DTM 5x5 2015 extracted from Geoportal of Lombardy Region (as the Digital Elevation Model (DEM) for topographic removal) and the mean daily temperature corresponding to scene acquisition (for estimation of thermal fluctuations).

According to the archive of levelling measurements obtained within the network of Como Cathedral, available at the repository of the Survey Department of Politecnico di Milano, high-precision levelling surveys were started in November 1985 on 46 benchmarks inside and outside the cathedral, which were followed by installation and measuring more benchmarks in the nearby area. With almost annual campaigns, the surveys have been carried out until May 2012. Due to the practical availability of CSK SAR images from 2010 over this area and, at the same time, the aim of this study, only the measurements acquired in the last three levelling campaigns (12 Apr 2010, 18 Apr 2011, 09 May 2012) have been employed to determine the vertical deformation rate at the benchmarks at which the measurement has been performed in all these three surveys (Figure 1(a)).

Property	Dataset	
Orbit Track	Ascending	Descending
Num. of SLC	44	44
Time Interval	05-Jun-2010 25-May-2012	26-Apr-2010 17-May-2012
Incident Angle [°]	29.34	26.69
Heading Angle [°]	191.19	348.49

Table 1. Characteristics of SAR images

3. METHODOLOGY

3.1 MT-DInSAR processing

In the context of DInSAR, one of the most challenging components which acts like an obstacle in the proper estimation of useful information is the atmospheric artefacts. One of the effective ways to remove this component is to use the PSP technique in order to, first, estimate and then remove the atmospheric phase screen (APS) from the whole scene. The alternative approach, which is implemented in this study, to tackle this issue is to limit the scene under study by focusing on the small portion containing the interested targets instead of processing the whole scene. The basic assumption is that the atmospheric delay is spatially uniform over this selected area, therefore, the differential phase between any arbitrary PS and reference point does not include the atmospheric component. This "Small Area" idea can significantly decrease the processing cost and can be effective when a single CH building and nearby surrounding site are concerned. However, it is important to check the validity of the assumption by controlling the outcomes.

Selecting a set of pixels as Persistent Scatterer Candidates (PSC), which are characterized by high quality in terms of being a good target for SAR sensors, is an initial step in a standard PS-InSAR. Firstly, it is done by neglecting the pixels which are detected as sidelobes around the pixels with a strong signal called Local Maxima (LM). Then, among these selected LMs, a second criterion is applied to sort out the best candidates, and this criterion can be chosen based on the value of parameters such as Amplitude Dispersion D_A, Amplitude Stability Index I_{AS}, and/or Spatial Coherence γ_{spt}. Through this cancelling-out procedure which aims at decreasing the processing time and obtaining more reliable information, several points with the potential of representing valuable information will be neglected.

Hence, in this study, a full-resolution perspective (considering all the pixels in the scene) has been considered to determine the potential of these commonly-neglected pixels in terms of estimated information. Here, due to utilizing the Small Area approach, the computational expenses are hammered, and thanks to Temporal Coherence γ_{tmp} (as one of the most crucial outcomes of MT-PS processing indicating the integrity and quality of estimated information at the corresponding pixel), the unreliable measurement points can be detected and then cancelled out. This can significantly increase the spatial distribution of points with reliable information in the matter of the real height of the targets (which is beneficial for 3D reconstruction of CH), seasonal fluctuations (showing the effect of climate change all over the CH), and displacement velocity.

Another important aspect is a proper selection of the image connection graph by which the SAR images are connected to establish the interferometric pairs in an MT approach, and each connection is characterized by a mean interferometric coherence γ_{int}. A standard PS-InSAR analysis works with a single master configuration (namely STAR graph), while other approaches such as Small-Baseline Subset (SBAS) (Berardino et al., 2002; Lanari et al., 2004) use redundant multiple connections (and sometimes full graph of connections in the case of QPS). Both configurations, besides other possible connection graphs, are available in the SARPROZ software package. Here, considering the full-resolution perspective, two processing techniques have been performed:

- T_{FPS}: Using a single master configuration with a STAR graph, and the master has been selected in the way of optimizing the values of the perpendicular (normal) β_n and temporal β_t baselines.
- T_{MQP}: limiting the values of γ_{int}, β_n, and β_t in a full graph configuration; and then, weighting the remained connections with mean γ_{spt} calculated in a $n \times n$ window centred at the pixel under processing.

The latter is mainly used in the case of Distributed Scatterer (DS) processing (such as QPS), through which the phase time series of weak pixels, being placed in a neighbourhood of similar pixels, is enhanced utilizing different techniques, such as spatial phase filtering or phase model estimation (Even and Schulz, 2018). This approach is commonly employed for non-urban areas with non-complex surfaces and particular applications such as landslide detection and monitoring. However, in the case of built ACH with particular geometric complexity, using this procedure may lead to undesirable results. Thus, the phase enhancement in T_{MQP} is not performed in this work and the phase time series are directly called from the unfiltered, spatially wrapped, and weighted interferograms for MT-PS Processing (similarly as T_{FPS}).

3.2 Vertical Displacement Extraction

Regarding precise levelling data, the time series obtained by the last three campaigns were already the vertical displacement of the benchmarks concerning the reference point located at the front entrance of the building. In order to obtain the annual vertical displacement rate (R_{DL}), here, a Least-Squares (LS) linear curve fitting is performed. On the other hand, the displacement velocities obtained by DInSAR are in the direction of Line Of Sight (LOS) corresponding to the viewing geometry and look angle (with respect to the nadir) of satellite imagery.

Different studies have been carried out to extract the 3D displacement component of the sensed ground target from LOS Velocity (v_{LOS}) (Pepe and Calò, 2017). One branch uses external displacement information, such as GNSS (Susaki et al., 2020) and GPS (Polcari et al., 2016). On the other hand, the data-driven approaches are devoted to the extraction of Up-Down (d_V), East-West (d_{EW}), and North-South (d_{NS}) components in a multi-track and multi-angle approach (using both ascending and descending from different satellites) considering their dependency on the viewing geometry and orbital parameters (Dai et al., 2015). An important issue in this branch is that most of the well-known satellites carrying SAR sensors are orbiting in a sun-synchronized near-polar track, which means that the azimuth direction is nearly parallel to the N-S direction, therefore, extracting d_{NS} is not relevant using data-driven approaches, and in this study, this component is neglected. Defining the projection trigonometry as

$$v_{LOS,i} = d_V \cos\theta_i - d_{EW} \sin\theta_i \cos\alpha_i \quad (1)$$

where θ and α are the incident angle and satellite heading angle (with respect to the north), respectively, only two points with different satellite parameters is enough to retrieve the unknown displacement rates. In Equation (1), depending on whether ascending or descending data stacks from on satellite mission are used, i corresponds to ascending or descending.

Due to the full-resolution perspective considered in this study, besides the meter-level-accuracy estimation of the height and rough positioning of the data points, a localized approach is implemented here through which a 3D portion is considered and all the data points falling within this space are involved in the extraction of displacement components. Therefore, when using ascending and descending data stacks acquired by constellations of a single satellite mission, for an arbitrary 3D portion Ω_3 including N and M InSAR-derived data points from ascending and descending datasets, respectively, the matrix version of Equation (1) can be stated as:

$$\begin{bmatrix} \cos\theta_a & \sin\theta_a \cos\alpha_a \\ \vdots & \vdots \\ \cos\theta_d & \sin\theta_d \cos\alpha_d \\ \vdots & \vdots \end{bmatrix}_{(N+M)\times 2} \begin{bmatrix} d_V \\ d_{EW} \end{bmatrix}_{2\times 1} = \begin{bmatrix} v_{LOS,a,j} \\ \vdots \\ v_{LOS,d,k} \\ \vdots \end{bmatrix}_{(N+M)\times 1} \quad (j = 1, \dots, N \text{ and } k = 1, \dots, M) \quad (2)$$

Each equation in this over-determinate linear system corresponds to a data point, which is characterized by temporal coherence γ_{tmp} showing the quality of the information estimation. Furthermore, despite the complex geometry of the building under study, it is assumed that in a localized space, the neighbouring data points falling within the Ω_3 make a planar surface. Hence, the absolute distance Δ_{pp} of each data point from the fitted planar surface in the Ω_3 is used as an identifier for spatial integrity of the data points. Here, a diagonal weight matrix composed of the contributions from $\gamma_{tmp}$and Δ_{pp} for an arbitrary Ω_3 is utilized:

$$\mathbf{W} = \mathbf{I}_{(N+M)} \odot \begin{bmatrix} \left(\frac{\max(\Delta_{pp})}{\Delta_{pp,a,j}}\right)\left(\frac{1}{\gamma_{tmp,a,j}}\right)^{-\rho} \\ \vdots \\ \left(\frac{\max(\Delta_{pp})}{\Delta_{pp,d,k}}\right)\left(\frac{1}{\gamma_{tmp,d,k}}\right)^{-\rho} \\ \vdots \end{bmatrix}_{(N+M)\times 1} \quad (3)$$

where $\mathbf{I}$ is the identity matrix, $\odot$ is the matrix-to-vector Hadamard (elementwise) product, and $\rho \geq 0$ is the influence power of the temporal coherence in the weighting procedure. Assuming that Equation (2) is expressed as $\mathbf{S}.\mathbf{d} = \mathbf{v}$, the LS method can be used to solve the weighted over-determinate linear system of

$$\mathbf{W^T}.\mathbf{W}.\mathbf{S}.\mathbf{d} = \mathbf{v} \quad (4)$$

and the deformation components of the interested 3D portion are retrieved. In the case that there are less than 4 data points within Ω_3, the component related to Δ_{pp} will be equal to 1, since the minimum points required for LS planar surface fitting is 4 points. The effectiveness of this weighting procedure will be discussed in Subsection 4.2.

The procedure described above is suitable for Ω_3 within which there are at least one data point from each ascending and descending dataset. A simplified method can be adopted to retrieve the vertical component of the LOS velocity which assumes that the E-W component is negligible, as well as N-S contribution. Therefore, for an arbitrary Ω_3, from Equation (1), it can be concluded that

$$d_V = v_{LOS,i} \,/\, \cos\theta_i \qquad (5)$$

This simplification of LOS projection is successfully used by different researchers (Bayramov et al., 2021) and has been also adopted in this study.

3.3 Validation Stages

The benchmarks for levelling operations have been placed on the ground level. Due to the viewing characteristics of satellite SAR imagery and the height of the buildings in the area of study, most of the levelling benchmarks and the corresponding nearby neighbourhood close to ground level are not simultaneously covered by both ascending and descending tracks. Hence, after merging ascending and descending InSAR-derived datasets, two major stages for the validation process are employed:

i) using simplified cosine correction of LOS velocity (Equation (5)) for the data points falling within Ω_3 defined by a circular buffer of 5-meter geodesic radius cantered at levelling benchmark and a height interval of [199-208] meters above sea level (asl) forming a cylinder-shaped space; then obtaining the weighted average of vertical velocity at each height sub-interval. Here, for weighting, the value of d_V of each data point is multiplied by the corresponding $(\gamma_{tmp})^{\rho}$ where $\rho = 5$ is chosen.

ii) Using the weighted multi-track displacement components extraction (Equation (4)) for the data points falling within Ω_3 defined by a circular buffer of 5-meter geodesic radius XY-cantered at levelling benchmark and Z-centered at a series of height values starting from 199 m asl to the highest value of height over the area of study with a spacing step of 1 m. The height of each cylinder-shaped Ω_3 is considered 1 m. It is important to note that the quantities of d_V in this stage are derived by previously weighted equations.

In each stage, the value of d_V for each Ω_3 is compared to vertical the displacement rate R_{DL} of the corresponding levelling benchmark in terms of absolute error.

4. RESULTS AND DISCUSSIONS

4.1 Preliminary Challenges, Solutions, and Results

After cropping and co-registration of both ascending and descending SAR images, the stacks have been manually geocoded, and then two techniques T_{FPS} and T_{MQP} have been performed. From an InSAR processing point of view, the main encountered challenges and the implemented solutions in different steps are: 1) selection of Ground Control Point (GCP)

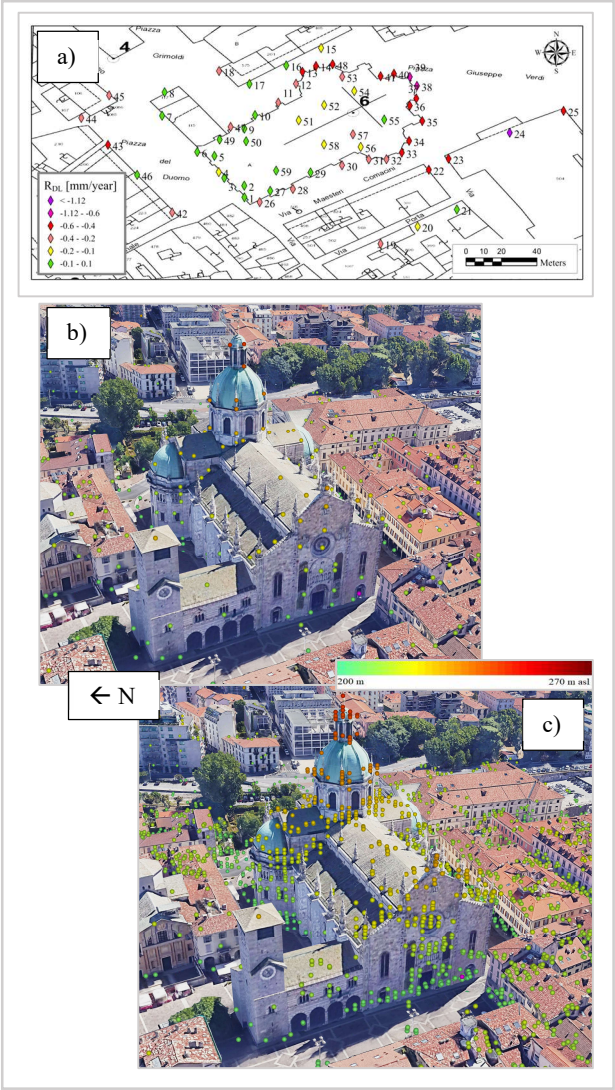

Figure 1. Area of interest: a) index and vertical displacement annual rate at each levelling benchmark, b) and c) Google Earth 3D building view, showing standard PS and T_{FPS} results, respectively, in terms of estimated height.

and the corresponding pixel in manual geocoding, which may result in a wrong estimation of residual height (with respect to the DEM) as a crucial component in DInSAR context. It was seen that choosing a GCP close to the building of interest may result in a more accurate estimation of information; 2) selection of Reference Point (RP) for MT PS processing, which may not affect the results where differential displacements are concerned. However, in cases such as comparison with the measurements obtained by other technologies (like this study), a wrong selection of RP can lead to very high values of the difference between the two techniques. Therefore, the closest InSAR data point to the RP of levelling measurements (Benchmark 1 in Figure 1(a)) is not necessarily the best option for RP of MT PS Processing (Purple point in Figure 1(b) and (c)); 3) validity evaluation of choosing Small Area hypothesis, which is done by checking if there are high-quality InSAR data points with high values of γ_{tmp} far from the selected RP. If so, basically, the atmospheric artefacts have not affected the differential phases between RP and the interested data point, which demonstrates the correctness of spatial uniformity of APS.

This contribution has been peer-reviewed. The double-blind peer-review was conducted on the basis of the full paper.
https://doi.org/10.5194/isprs-annals-X-M-1-2023-79-2023 | © Author(s) 2023. CC BY 4.0 License.

The threshold of Temporal Coherence $\gamma_{tmp} \geq 0.65$ is selected for all the InSAR results hereafter, meaning that the data points characterized by lower values of γ_{tmp} are neglected. The results of T_{FPS} are shown in Figure 1 (c), which are similar to the results of T_{MQP} in this level of interpretation. Figure 1(b) shows the results of a standard PS analysis after applying the Local Maxima criterion for PSC selection (neglecting sidelobes). Comparing (b) and (c) proves the significant enhancement in spatial density of data points which is beneficial for 3D reconstruction of ACH and point cloud generation and processing.

Recalling, once again, the necessity of evaluation of the information estimation quality through DInSAR, the deformation trend (velocity in mm per year) parameter obtained by different techniques is discussed in the next subsection.

4.2 Validation outcomes

Following the strategy developed in subsection 3.3, the outcome of Validation stage (i) is shown in Figure 2 (a) and (b) respectively for T_{FPS} and T_{MQP}. Here, the points which could be chosen as Local Maxima (LM) are excluded from the full-resolution analysis, and Sidelobes (SL) and ML points have been assessed separately. As mentioned previously, the $\Omega_3$blocks in this stage are Z-cantered at different heights (forming several subintervals) at each benchmark. The weighted average absolute errors at each Ω_3 (excluding LM points) are shown with the times-sign-shaped data points, while the mean value of all the subinterval errors is shown with diamond blue

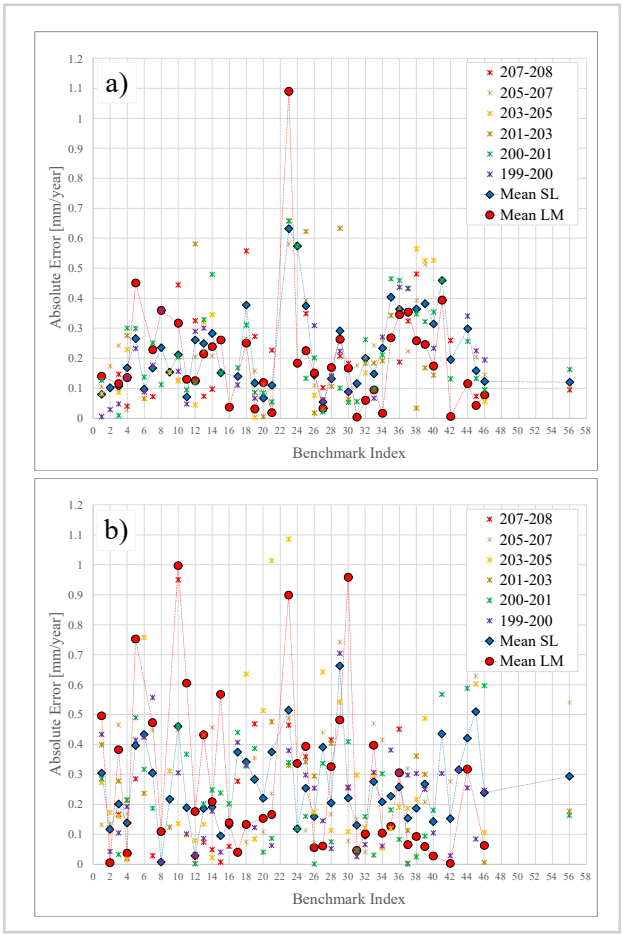

Figure 2. Validation stage (i) with absolute errors (weighted average) for different types of data point and height subintervals: a) T_{FPS} and b) T_{MQP}

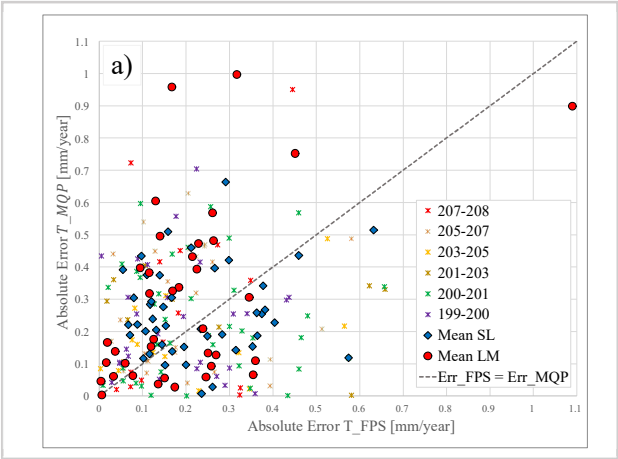

Figure 3. The correlation between T_{FPS} and T_{MQP} absolute errors

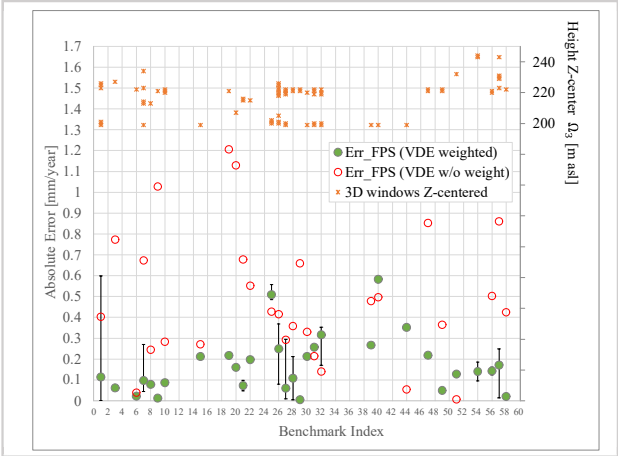

Figure 4. Validation stage (ii) absolute errors (weighted average) based on $T_{FPS}$and Z-center height of available Ω_3 at each benchmark.

shapes. The weighted average of ML absolute error is shown with the red circle.

At first glance, it is obvious that except for some rare violations, the errors are approximately limited to 0.6 [mm/year] for both employed DInSAR techniques. Inspecting the dense concentration of errors, from a statistical point of view, this approximate limit goes down to 0.3 and 0.5 [mm/year] for T_{FPS} and T_{MQP}, respectively. Furthermore, Figure 3, illustrating the correlation between the errors in both techniques, shows that the T_{FPS} is more realistic than T_{MQP} when processing the ML pixels (low number of red circles at the right side of the dashed grey line). Such a claim can barely be made for mean SL points based on Figure 3, since these types of data points have different deformation detection capabilities at different benchmarks. However, considering the expensive processing time for T_{MQP} due to a higher number of interferometric pairs (sometimes 10 times more with respect to T_{MQP}) and calculation of spatial coherence for interferogram weighting through DInSAR processing, and also by considering the denser concentration of mean SL data points in Figure 2(a) close to zero, it can be concluded that T_{FPS} is a better option with higher performance for exploiting the full-resolution potential of SAR images in this class of applications.

Since then, the validation outcomes have been concerning the simplified cosine correction of LOS velocity (Equation (5)). On

the performance of weighted localized Vertical Displacement Extraction (VDE) (Equation (4)), Figure 4 shows the absolute errors in the case of using VDE with and without weighting (taking advantage of γ_{tmp} and Δ_{pp} if available) in the benchmarks where this type of VDE is possible at one or multiple Ω_3 blocks. Comparing hollow red circles with filled green points, weighting may increase the errors by a very small amount in a few instances, however, the several significant drops from very high values of the error to lower values of 0.3 [mm/year] through weighted VDE is remarkable. Similar to Figure 2(a), the dense concentration of errors using weighted VDE can be seen at values lower than 0.3 [mm/year] which reveals the high quality of the detected displacements. Most of the Ω_3 are Z-centred at approximately 220 [m asl] at (or close) to the edges of the main roof (where the walls meet the first-level roof) approximately 20 meters upper than ground level. From benchmark 26 to 32 located on the southern side of the cathedral, almost all the Ω_3 can be found on ground level or at the 220-meter level. The InSAR-derived vertical velocity close to benchmarks 47 and 49 at the northern side of the building, which could not be assessed through the Validation stage (i), are representing very low values of errors while obtained 20 m higher than ground level. It is important to note that the InSAR-detected vertical velocities at benchmarks 54 and 57 installed on the ground level of interior columns holding the dome of the cathedral are estimated in Ω_3 located on the dome at the height of ca. 243 [m asl] with high precision. The same for interior benchmarks 51 and 58 can be mentioned, where Ω_3 are located on the main roof of the building.

Comparing the Validation stage (i) and (ii) where the Ω_3 blocks are Z-centred within the height interval of stage (i), it was seen that no correlation between absolute errors of the stage (i) and horizontal East-West velocities of the stage (ii) could be found, which means that the errors in simplified cosine correction of the stage (i) does not correspond to the presence of horizontal displacement.

5. CONCLUSIONS

In this work, Cosmo-SkyMed SAR images have been used to determine the vertical displacement rates of the Cathedral of Como, using different DInSAR algorithms and different vertical component extraction techniques. The performance of the algorithms and techniques in exploiting the potential of full-resolution perspective (using all the pixels in the SAR image) has been assessed by comparing the outcomes with high-precision levelling measurements acquired on the cathedral and nearby area. Different challenges and obstacles in the proper framework of InSAR analysis and validation are discussed in detail.

As the key outcome, the results showed that using a single-master configuration for DInSAR processing (T_{FPS} algorithm) is more efficient in terms of higher accuracy and lower processing time. In this case, the simplified cosine correction of LOS velocities shows reasonable results, and the observed errors may not be affected by possible horizontal movements. Using both temporal coherence and the distance from the fitted planar surface in the localized block as the weight of the Localized Vertical Displacement Extraction procedure can significantly decrease the high values of error in such a framework of validation.

Besides the significant contribution of this work to the reliability assessment of InSAR displacement monitoring of cultural heritage by defining an accuracy level, the other parameters (such as residual height, seasonal fluctuations, and geographical positioning) estimated through DInSAR processing and post-processing are still required to be evaluated in such a reliable framework. This can be a prospective view for future study.

6. ACKNOWLEDGEMENT

The authors would like to acknowledge the Italian Space Agency (ASI) for delivering the Cosmo-SkyMed SAR images. The paper benefited from technical discussions with Dr. Alfredo Rocca regarding the InSAR processing, and the authors thank Dr. Daniele Perissin for providing SARPROZ software package used in this study for SAR and InSAR processing.

REFERENCES

Bajni, G., Apuani, T.,Beretta, G. P., 2019. Hydro-geotechnical modelling of subsidence in the Como urban area. Engineering Geology, 257, 105144.

Bayramov, E., Buchroithner, M., Kada, M.,Zhuniskenov, Y., 2021. Quantitative Assessment of Vertical and Horizontal Deformations Derived by 3D and 2D Decompositions of InSAR Line-of-Sight Measurements to Supplement Industry Surveillance Programs in the Tengiz Oilfield (Kazakhstan). 13, 2579.

Berardino, P., Fornaro, G., Lanari, R.,Sansosti, E., 2002. A new algorithm for surface deformation monitoring based on small baseline differential SAR interferograms. IEEE Transactions on geoscience remote sensing
40, 2375-2383.

Berto, L., Doria, A., Saetta, A., Stella, A.,Talledo, D., 2021. Assessment of the Applicability of DInSAR Techniques for Structural Monitoring of Cultural Heritage and Archaeological Sites. Proceedings, Civil Structural Health Monitoring, Cham, 691-697.

Bozzano, F., Ciampi, P., Del Monte, M., Innocca, F., Luberti, G. M., Mazzanti, P., Rivellino, S., Rompato, M., Scancella, S.,Scarascia Mugnozza, G., 2020. Satellite a-dinsar monitoring of the Vittoriano monument (Rome, Italy): implications for heritage preservation. Italian journal of engineering geology and environment, 2, 5-17.

Cavalagli, N., Kita, A., Falco, S., Trillo, F., Costantini, M.,Ubertini, F. J. R. S. o. E., 2019. Satellite radar interferometry and in-situ measurements for static monitoring of historical monuments: The case of Gubbio, Italy. 235, 111453.

Cavalagli, N., Kita, A., Farneti, E., Falco, S., Trillo, F., Costantini, M., Fornaro, G., Reale, D., Verde, S.,Ubertini, F., Remote Sensing and In-Situ Measurements for the Structural Monitoring of Historical Monuments: The Consoli Palace of Gubbio, Italy. Proceedings, European Workshop on Structural Health Monitoring, Cham, 119-128.

Chen, F., Lasaponara, R.,Masini, N., 2017. An overview of satellite synthetic aperture radar remote sensing in archaeology: From site detection to monitoring. Journal of Cultural Heritage, 23, 5-11.

Chen, F., Xu, H., Zhou, W., Zheng, W., Deng, Y.,Parcharidis, I., 2021. Three-dimensional deformation monitoring and simulations for the preventive conservation of architectural heritage: a case study of the Angkor Wat Temple, Cambodia. GIScience & Remote Sensing, 58, 217-234.

Chen, F., Zhou, W., Tang, Y., Li, R., Lin, H., Balz, T., Luo, J., Shi, P., Zhu, M.,Fang, C., 2022. Remote sensing-based deformation monitoring of pagodas at the Bagan cultural heritage site, Myanmar. International Journal of Digital Earth, 15, 770-788.

Costantini, M., Falco, S., Malvarosa, F.,Minati, F., A new method for identification and analysis of persistent scatterers in series of SAR images. Proceedings, IGARSS 2008-2008 IEEE

International Geoscience and Remote Sensing Symposium, II-449-II-452.

Crosetto, M., Monserrat, O., Cuevas-González, M., Devanthéry, N.,Crippa, B., 2016. Persistent scatterer interferometry: A review. ISPRS Journal of Photogrammetry and Remote Sensing, 115, 78-89.

Dai, K., Liu, G., Li, Z., Li, T., Yu, B., Wang, X.,Singleton, A., 2015. Extracting Vertical Displacement Rates in Shanghai (China) with Multi-Platform SAR Images. 7, 9542-9562.

Eskandari, R.,Scaioni, M., 2023. RETROSPECTIVE STUDY OF VERTICAL GROUND DEFORMATION IN COMO, NORTHERN ITALY: INTEGRATION OF LEVELLING AND PSI MEASUREMENTS. Int. Arch. Photogramm. Remote Sens. Spatial Inf. Sci., XLVIII-4/W2-2022, 31-38.

Even, M.,Schulz, K. J. R. S., 2018. InSAR deformation analysis with distributed scatterers: A review complemented by new advances. 10, 744.

Ferretti, A., Prati, C.,Rocca, F., 2000. Nonlinear subsidence rate estimation using permanent scatterers in differential SAR interferometry. IEEE Transactions on geoscience remote sensing 38, 2202-2212.

Ferretti, A., Prati, C.,Rocca, F., 2001. Permanent scatterers in SAR interferometry. IEEE Transactions on geoscience remote sensing
39, 8-20.

HO TONG MINH, D., Hanssen, R.,Rocca, F. J. R. S., 2020. Radar interferometry: 20 years of development in time series techniques and future perspectives. 12, 1364.

Karila, K., Karjalainen, M., Hyyppä, J., Koskinen, J., Saaranen, V.,Rouhiainen, P., 2013. A Comparison of Precise Leveling and Persistent Scatterer SAR Interferometry for Building Subsidence Rate Measurement. 2, 797-816.

Lanari, R., Mora, O., Manunta, M., Mallorquí, J. J., Berardino, P., Sansosti, E. J. I. t. o. g.,sensing, r., 2004. A small-baseline approach for investigating deformations on full-resolution differential SAR interferograms. 42, 1377-1386.

Lasaponara, R.,Masini, N.: Active Satellite Sensors in Cultural Heritage Research: The Use of SAR for Archaeological Prospection, in: Remote Sensing for Archaeology and Cultural Landscapes: Best Practices and Perspectives Across Europe and the Middle East, edited by: Hadjimitsis, D. G., Themistocleous, K., Cuca, B., Agapiou, A., Lysandrou, V., Lasaponara, R., Masini, N., and Schreier, G., Springer International Publishing, Cham, 107-121, 10.1007/978-3-030-10979-0_7, 2020.

Moise, C., Dana Negula, I., Mihalache, C. E., Lazar, A. M., Dedulescu, A. L., Rustoiu, G. T., Inel, I. C.,Badea, A., 2021. Remote Sensing for Cultural Heritage Assessment and Monitoring: The Case Study of Alba Iulia. 13, 1406.

Nappo, N., Ferrario, M. F., Livio, F.,Michetti, A. M., 2020. Regression Analysis of Subsidence in the Como Basin (Northern Italy): New Insights on Natural and Anthropic Drivers from InSAR Data. Remote Sensing, 12.

Nappo, N., Peduto, D., Polcari, M., Livio, F., Ferrario, M. F., Comerci, V., Stramondo, S.,Michetti, A. M., 2021. Subsidence in Como historic centre (northern Italy): Assessment of building vulnerability combining hydrogeological and stratigraphic features, Cosmo-SkyMed InSAR and damage data. International Journal of Disaster Risk Reduction, 56, 102115.

Pepe, A.,Calò, F., 2017. A Review of Interferometric Synthetic Aperture RADAR (InSAR) Multi-Track Approaches for the Retrieval of Earth’s Surface Displacements. Applied Sciences, 7, 1264.

Perissin, D.,Wang, T., 2012. Repeat-Pass SAR Interferometry With Partially Coherent Targets. IEEE Transactions on Geoscience and Remote Sensing, 50, 271-280.

Perissin, D., Wang, Z.,Wang, T., 2011. The SARPROZ InSAR tool for urban subsidence/manmade structure stability monitoring in China. Proceedings of the ISRSE, Sidney, Australia, 1015.

Polcari, M., Palano, M., Fernández, J., Samsonov, S. V., Stramondo, S.,Zerbini, S., 2016. 3D displacement field retrieved by integrating Sentinel-1 InSAR and GPS data: the 2014 South Napa earthquake. European journal of remote sensing, 49, 1-13.

Rudokas, K., Landauskas, M., Gražulevičiūtė-Vilneiškė, I.,Viliūnienė, O., 2019. Valuing the socio-economic benefits of built heritage: Local context and mathematical modeling. Journal of Cultural Heritage, 39, 229-237.

Scaioni, M., Marsella, M., Crosetto, M., Tornatore, V.,Wang, J., 2018. Geodetic and Remote-Sensing Sensors for Dam Deformation Monitoring. 18, 3682.

Susaki, J., Kusakabe, T.,Anahara, T., 2020. ESTIMATING 3D LAND SUBSIDENCE FROM MULTI-TEMPORAL SAR IMAGES AND GNSS DATA USING WEIGHTED LEAST SQUARES. ISPRS Annals of the Photogrammetry, Remote Sensing and Spatial Information Sciences, V-3-2020, 165-172.

Tapete, D.,Cigna, F., 2017a. Trends and perspectives of space-borne SAR remote sensing for archaeological landscape and cultural heritage applications. Journal of Archaeological Science: Reports, 14, 716-726.

Tapete, D.,Cigna, F., 2017b. InSAR data for geohazard assessment in UNESCO World Heritage sites: state-of-the-art and perspectives in the Copernicus era. International Journal of Applied Earth Observation and Geoinformation, 63, 24-32.

Tapete, D.,Cigna, F., 2019. COSMO-SkyMed SAR for Detection and Monitoring of Archaeological and Cultural Heritage Sites. 11, 1326.

Tapete, D., Cigna, F., Masini, N.,Lasaponara, R. J. A. P., 2013. Prospection and monitoring of the archaeological heritage of Nasca, Peru, with ENVISAT ASAR. 20, 133-147.

Tapete, D., Fanti, R., Cecchi, R., Petrangeli, P.,Casagli, N., 2012. Satellite radar interferometry for monitoring and early-stage warning of structural instability in archaeological sites. Journal of Geophysics and Engineering, 9, S10-S25.

Themistocleous, K., Cuca, B., Agapiou, A., Lysandrou, V., Tzouvaras, M., Hadjimitsis, D. G., Kyriakides, P., Kouhartsiouk, D., Margottini, C., Spizzichino, D., Cigna, F., Crosta, G., Frattini, P.,Merodo, J. A. F., The Protection of Cultural Heritage Sites from Geo-Hazards: The PROTHEGO Project. Proceedings, Digital Heritage. Progress in Cultural Heritage: Documentation, Preservation, and Protection, Cham, 91-98.

Tzouvaras, M., Kouhartsiouk, D., Agapiou, A., Danezis, C.,Hadjimitsis, D. G., 2019. The Use of Sentinel-1 Synthetic Aperture Radar (SAR) Images and Open-Source Software for Cultural Heritage: An Example from Paphos Area in Cyprus for Mapping Landscape Changes after a 5.6 Magnitude Earthquake. 11, 1766.

Werner, C., Wegmuller, U., Strozzi, T.,Wiesmann, A., Interferometric point target analysis for deformation mapping. Proceedings, IGARSS 2003. 2003 IEEE International Geoscience and Remote Sensing Symposium. Proceedings (IEEE Cat. No. 03CH37477), 4362-4364.

Wojtkowska, M., Kedzierski, M.,Delis, P., 2021. Validation of terrestrial laser scanning and artificial intelligence for measuring

deformations of cultural heritage structures. Measurement, 167, 108291.

Yang, X., Wang, D., Xu, Y., Hou, M.,Wang, Z., 2022. Performance Assessment of InSAR-Based Vertical Displacement Monitoring of Sluices in Coastal Soft Soil Area. KSCE Journal of Civil Engineering, 26, 371-380.